International Journal of Fracture, **57**, 1–24 (1992).

The Initiation and Growth of Delaminations Induced by Matrix Microcracks in Laminated Composites

J. A. NAIRN and S. HU

Department of Materials Science and Engineering,

University of Utah, Salt Lake City, Utah 84112, USA

Submitted January 27, 1992, Accepted 1992

Abstract. A recent variational mechanics analysis of microcracking damage in cross-ply laminates of the form $[(S)/90_n]_s$, where (S) is any orthotropic sublaminate much stiffer than $[90_n]$, has been extended to account for the presence of delaminations emanating from the tips of microcracks in the $[90_{2n}]_T$ sublaminate. The new two-dimensional stress analysis is used to calculate the total strain energy, effective modulus, and longitudinal thermal expansion coefficient for a laminate having microcracks and delaminations. These results are used to calculate the energy release rate for the initiation and growth of a delamination induced by a matrix microcrack. At low crack densities, $[(S)/90_n]_s$ laminates are expected to fail by microcracking and to show little or no delamination. At some critical crack density, which is a function of laminate structure and material properties, the energy release rate for delamination exceeds that for microcracking and delamination is predicted to dominate over microcracking. A quasi-three-dimensional model is used to predict the propagation of arbitrarily shaped delamination fronts. All predictions agree with experimental observations.

1. Introduction

Interaction between microcracking and delamination is well illustrated by the case study of $[\pm 25/90_n]_s$ laminates for $n = \frac{1}{2}$, 1, 2, 3, 4, 6, and 8 [1–4]. With the exception of the $n = \frac{1}{2}$ laminate, the initial form of damage is microcracking in the 90° ply groups. Laminates with $n \leq 3$ show thumbnail shaped edge delaminations along the laminate midplane. In the presence of microcracks these edge delaminations sometimes divert to the $-25/90$ interface. Laminates with $n \geq 4$ show delaminations at the $-25/90$ interface emanating from the tips of existing microcracks. The microcrack induced delaminations initiate at the free edge and spread into the laminate along the microcrack tips. The number of microcracks formed before the onset of delamination decreases as n increases (for $n \geq 4$). This paper presents a new analytical technique for predicting the initiation and propagation of these microcrack induced delaminations. The predictions agree with experimental observations [1–4].

Hashin used variational mechanics techniques to derive an approximate stress analysis for cross-ply laminates having microcracks in the 90° plies [5–8]. Nairn *et. al.* extended Hashin's analysis to include residual thermal stresses and to calculate energy releases rates for the formation of new microcracks [9,10]. Using critical energy release rate as a failure criterion has been powerful in predicting the formation and growth of microcracking damage in cross-ply laminates during static loading [9,10], fatigue loading [11], and

thermal cycling [12]. In this paper we extend the variational analysis to account for delaminations emanating from the tips of existing microcracks. The basic analysis is two-dimensional. We can draw some conclusions about three dimensional effects by constructing a quasi-three-dimensional model from the two-dimensional analysis results.

Considering the importance of delamination damage, there have been limited efforts at explaining microcrack induced delaminations. O'Brien [13,14] developed the first analytical method for the energy release rate associated with the growth of microcrack induced delaminations by using simple load sharing rules. In regions adjacent to delaminations, the 90° plies are assumed to carry no load and thus the uncracked plies carry proportionately increased loads. In regions where there is no delamination, the stresses in all plies are identical to the stresses in the undamaged state. The resulting energy release rate is independent of delamination size and has been shown in subsequent calculations to be in reasonable agreement with three-dimensional finite element analysis [15]. O'Brien's result will be shown to be a limiting special case of the variational analysis that applies to delaminations induced by isolated microcracks. Experimental observations show that microcrack induced delaminations usually do not appear until after the formation of many microcracks [1,4]. Thus, instead of analyzing delaminations induced by isolated microcracks, it is important to consider delaminations induced by microcracks in the proximity of neighboring microcracks. The new variational analysis is capable of accounting for the effect of neighboring microcracks and the effect can be significant.

Dharani and Tang [16] describe a consistent shear-lag theory analysis for both microcracking and microcrack induced delaminations. They predict failure using numerical stress calculations and a point-stress failure criterion. Many of their predictions are in qualitative agreement with experimental results. Like O'Brien's analysis [13,14], however, Dharani and Tang's delamination study is limited to delamination at isolated microcracks.

Several authors describe three-dimensional finite element analyses of free-edge and microcrack induced delaminations [15,17,18]. Fish and Lee [17] consider delaminations near the free edge that are inclined 45° with respect to the microcrack. The crack shape they assume is reasonable for free-edge delaminations in the absence of microcracks but is not a good representation of microcrack induced delaminations (see Refs. [1] and [4]). Wang *et. al.* [18] assume a specific delamination growth process and calculate the energy released as the delamination grows. Because they assume a specific growth process, their results are only useful in a qualitative sense. Salpekar and O'Brien [15], describe the most comprehensive results including 45° inclined crack fronts, 10.6° inclined crack fronts, and through-the-width delaminations. They calculated mode I, mode II, and mode III energy release rates as a function of position along the various crack fronts. In general, the three-dimensional finite element analyses provide important information about edge effects that can not be learned from two-dimensional or quasi-three-dimensional analysis. Their practical utility is limited, however, because by restricting the models to isolated microcracks they fail to account for the effect of neighboring microcracks.

This paper begins with a two-dimensional variational analysis of a microcrack induced through-the-width delamination. We derive an approximate stress state which is subsequently used to calculate a closed form analytical solution of the energy release rate for the propagation of a delamination emanating from an existing microcrack tip. The analysis explicitly accounts for residual thermal stresses and neighboring microcracks.

We obtain information about three-dimensional effects by constructing a quasi-three-dimensional model based on the two-dimensional analysis and lumped spring elements. In the results section we discuss the competition between microcracking and delamination failure modes, the growth of a delamination in the proximity of neighboring microcracks, and the three-dimensional effects on the shape of the delamination crack front. All predictions agree with experimental observations (see Refs. [1] and [4]). Finally, we discuss the accuracy of the variational analysis and conclude it to be similar to the accuracy of beam theories for delamination.

2. Two-Dimensional Stress Analysis

Consider the initiation and growth of a delamination emanating from an existing microcrack that spans the cross section of the 90° plies in a model laminate of construction $[(S)/90_n]_s$, where (S) is any orthotropic sublaminate. We begin with a two-dimensional analysis of a damaged sample under a uniform and uniaxial applied stress σ_0 in the x direction. Assuming that (S) is a relatively stiff sublaminate (such as $[0_m]$ or $[(\pm\theta)_m]$ with $\theta < 45°$) and that n is not too small (*e.g.* $n \geq 2$), the initial form of damage will be matrix microcracking in the 90° plies. Before any microcracks induce delaminations at the $(S)/90°$ interface, the laminate will appear as in Fig. 1A. Figure 1B shows a representative element of damage from Fig. 1A as the space between two existing microcracks separated by a distance $2a$. Upon continued loading any of the microcracks may induce a delamination at the $(S)/90°$ interface. Figure 1C shows the formation of delaminations of lengths d_1 and d_2 emanating from the top and bottom microcracks of the representative element of damage. Our stress analysis is for the element of damage in Fig. 1C and thus we only show the delaminations within that element. Naturally delaminations may propagate above or below the element of damage, but such delaminations do not affect the subsequent stress analysis. To preserve symmetry, we assume equal delamination lengths on either side of the $[90_{2n}]_T$ sublaminate. The stress analysis goal is to solve for the stresses and the total strain energy in the representative element of damage as a function of microcrack spacing and delamination lengths.

2.1. An Admissible Stress State

By virtue of symmetry, we only need to analyze the right half of the symmetric element in Fig. 1C. We indicate the $[90_n]$ sublaminate from $z = 0$ to $z = t_1$ with superscript (1) and the (S) sublaminate from $z = t_1$ to $z = t_2$ with superscript (2). We split the zone between the two existing microcracks into three regions. Region I is the one within the top delamination or the region from $x = a - d_1$ to $x = a$. Region II is the one between the tips of the delaminations or the region from $x = -a + d_2$ to $x = a - d_1$. Region III is the one within the bottom delamination or the region from $x = -a$ to $x = -a + d_2$ (see Fig. 1C).

We make one and only one assumption about the stresses — that the x axis tensile stresses within the $[90_n]$ sublaminate and within the (S) sublaminate are independent of thickness or z direction and depend only on x. This assumption was introduced by Hashin [5,6] and used by others [9,10] in variational mechanics analysis of microcracking damage. From Hashin [5], the only possible stress state obeying the assumption

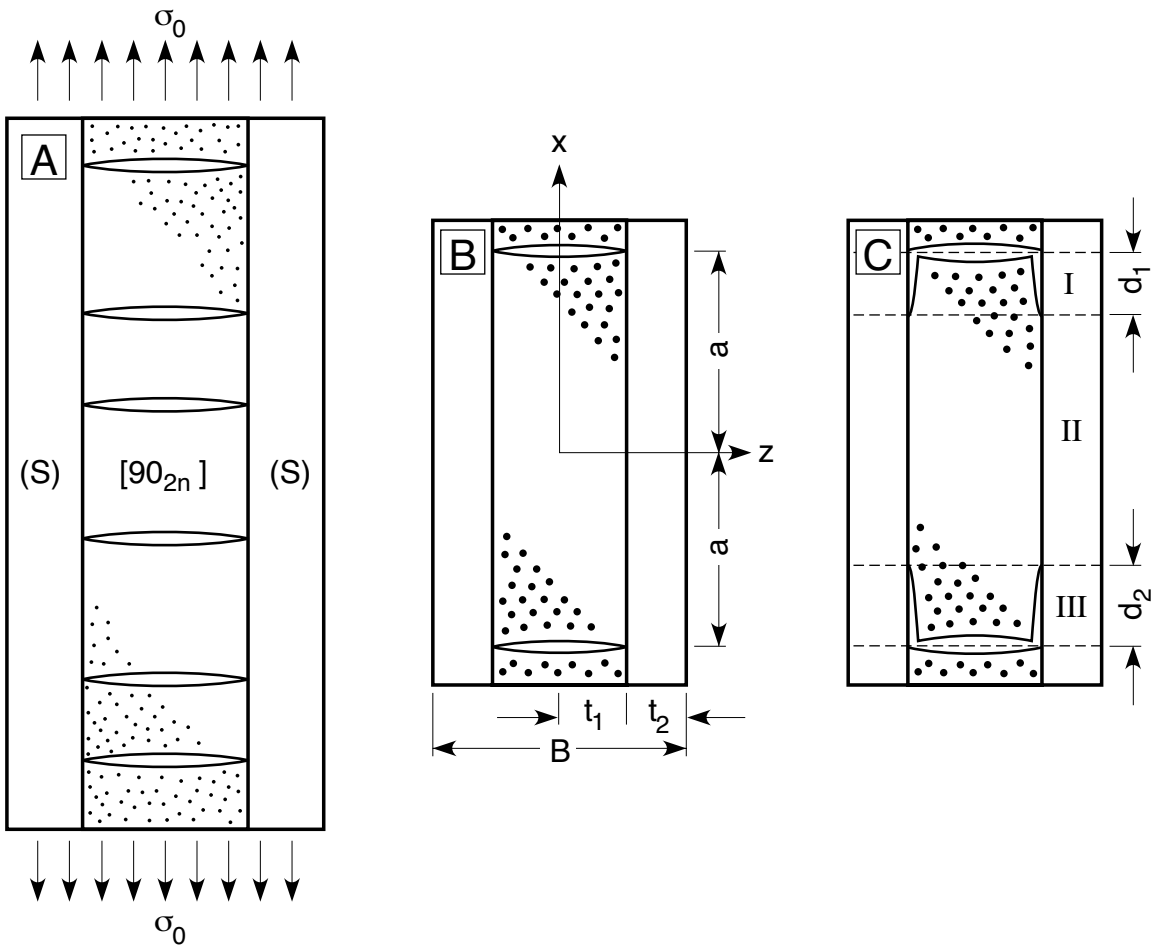

Figure 1: A. An edge view of a $[(S)/90_n]_s$ laminate having several microcracks in the 90° plies. B. A representative element of damage which is the space between two microcracks separated by a distance of $2a$. C. The same representative element of damage after delaminations of lengths d_1 and d_2 have propagated from the microcrack tips.

that simultaneously satisfies equilibrium and traction boundary conditions is [5,9]:

$$\begin{aligned} \sigma_{xx}^{(1)} &= \sigma_{x0}^{(1)} - \psi(x) \qquad & \sigma_{xz}^{(1)} &= \psi'(x)z \qquad & \sigma_{zz}^{(1)} &= \frac{1}{2}\psi''(x)(ht_1 - z^2) \\ \sigma_{xx}^{(2)} &= \sigma_{x0}^{(2)} + \frac{\psi(x)}{\lambda} \qquad & \sigma_{xz}^{(2)} &= \frac{\psi'(x)}{\lambda}(h-z) \qquad & \sigma_{zz}^{(2)} &= \frac{\psi''(x)}{2\lambda}(h-z)^2 \end{aligned} \tag{1}$$

where $\lambda = \frac{t_2}{t_1}$ and $\sigma_{x0}^{(1)}$ and $\sigma_{x0}^{(2)}$ are the initial stresses or the stresses in a laminate that has no damage and is at the stress-free temperature. By an equal strain condition

$$\sigma_{x0}^{(1)} = \frac{E_x^{(1)}}{E_c}\sigma_0 \qquad \text{and} \qquad \sigma_{x0}^{(2)} = \frac{E_x^{(2)}}{E_c}\sigma_0 \tag{2}$$

where $E_x^{(i)}$ is the x direction Young's modulus of sublaminate i and E_c is the x direction Young's modulus of the undamaged laminate. The function $\psi(x)$ in Eq. (1) is the perturbation x axis tensile stress or the change in tensile stress caused by the formation of damage and the imposition of thermal loading. Due to the one assumption in the analysis, $\psi(x)$ is only a function of x. The solution for the stresses in the microcracked

and delaminated element involves determining $\psi(x)$ in each region (see Fig. 1C). The boundary conditions for $\psi(x)$ are

$$\psi(\pm a) = \sigma_{x0}^{(1)} \tag{3}$$

$$\psi'(\pm a) = 0 \tag{4}$$

$$\psi''(x) = \psi'(x) = 0 \quad \text{for} \quad a - d_1 < x < a \quad \text{and for} \quad -a < x < -a + d_2 \tag{5}$$

The first two boundary conditions provide traction free surfaces on the matrix microcracks and the last provides traction free surfaces on the delaminations.

2.2 Stress States in Regions I and III

The boundary conditions in regions I and III require $\psi'(x) = 0$. Integrating $\psi'(x)$ implies that $\psi(x)$ is constant. By Eq. (3) we have $\psi = \sigma_{x0}^{(1)}$ throughout regions I and III. Substituting $\psi(x)$ into Eq. (1) yields the region I and III stress states:

$$\begin{aligned} &\sigma_{xx}^{(1)} = 0 && \sigma_{xx}^{(2)} = \sigma_{x0}^{(2)} + \frac{\sigma_{x0}^{(1)}}{\lambda} = \frac{1+\lambda}{\lambda}\sigma_0 \\ &\sigma_{xz}^{(1)} = \sigma_{zz}^{(1)} = 0 && \sigma_{xz}^{(2)} = \sigma_{zz}^{(2)} = 0 \end{aligned} \tag{6}$$

The stresses in the $[90_n]$ sublaminate in regions I and III are zero. The constant and uniaxial stress state in the (S) sublaminate receives the load no longer carried by the $[90_n]$ sublaminate. The simple stress state in Eq. (6) is the only admissible stress state that satisfies the assumption of $\sigma_{xx}^{(i)}$ being independent of z as well as satisfying all boundary conditions. The exact solution would certainly show variations from a simple uniaxial stress state, but we expect that globally this stress state provides an acceptable approximation for the total strain energy in regions I and III.

Integrating the strain energy density over regions I and III for a sample of width W (y direction sample dimension) gives the total strain energy in regions I and III as

$$U_{I+III}(\delta) = 2W\left(\int_{-a}^{-a+d_2} dx \int_{t_1}^{\frac{B}{2}} dz \frac{{\sigma_{xx}^{(2)}}^2}{2E_x^{(2)}} + \int_{a-d_1}^{a} dx \int_{t_1}^{\frac{B}{2}} dz \frac{{\sigma_{xx}^{(2)}}^2}{2E_x^{(2)}}\right) = \frac{\sigma_0^2}{2E_x^{(2)}} \frac{1+\lambda}{\lambda} 2\delta t_1 BW \tag{7}$$

where we have introduced a dimensionless average delamination length, δ, defined as

$$\delta = \frac{d_1 + d_2}{2t_1} \tag{8}$$

2.3 Stress State in Region II

Because the stresses in the $[90_n]$ sublaminate of regions I and III are zero, that section of the $[90_n]$ sublaminate can be removed from the sample with no effect on the stress states. Removing the region I and III $[90_n]$ sublaminates effectively replaces the two microcracks by rectangular cut outs of length d_1 and d_2. With rectangular cut outs, there are stress-free fracture surfaces at the top and bottom of region II. The stress analysis of region II is thus identical to the stress analysis of a representative element of damage that has no delaminations (see Fig. 1B) but has two microcracks separated by $2a - d_1 - d_2$. Hashin [5,6] used variational mechanics to derive an approximate but reasonably accurate solution for the stresses between two existing microcracks in a $[0_m/90_n]_s$ laminate. His analysis for stress state was extended by Nairn *et. al.* [9,10] to include residual thermal stresses. In the appendix we summarize the previous variational mechanics analyses and extend them to include the more general $[(S)/90_n]_s$ laminate. The stress state in region II follows from $\psi(\xi)$ which is found by minimizing the total complementary energy. The result is

$$\psi(\xi) = \left(\sigma_{x0}^{(1)} - \frac{\Delta\alpha T}{C_1}\right)\phi(\xi) + \frac{\Delta\alpha T}{C_1} \tag{9}$$

where $\Delta\alpha = \alpha_x^{(1)} - \alpha_x^{(2)}$ is the difference between the x direction thermal expansion coefficients of the two sublaminates, $T = T_s - T_0$ is the difference between the sample temperature T_s, and the residual stress free temperature T_0, C_1 is a material constant, and $\phi(\xi)$ is a function of the dimensionless variable, ξ, defined as

$$\xi = \frac{2x - d_2 + d_1}{2t_1} \tag{10}$$

C_1 and $\phi(\xi)$ depend on the dimensions and material properties of the laminate and are defined in the appendix. In the dimensionless coordinate, the top and bottom microcracks are located at $\xi = \pm(\rho - \delta)$ where

$$\rho = \frac{a}{t_1} \tag{11}$$

In other words, when ρ is the dimensionless half spacing between the existing microcracks in Fig. 1C, the stresses in region II are identical to the stresses in Fig. 1B when the dimensionless half spacing between the existing microcracks is $\rho - \delta$.

Integrating the strain energy density in region II (see appendix), the total strain energy for region II in a sample of width W is

$$U_{II}(\rho,\delta) = \left(\frac{\sigma_0^2}{2E_c} + \frac{t_1\Delta\alpha^2T^2}{C_1B}\right)2(\rho-\delta)t_1BW + 2C_3t_1^2\chi(\rho-\delta)W\left(\frac{{E_x^{(1)}}^2}{E_c^2}\sigma_0^2 - \frac{\Delta\alpha^2T^2}{C_1^2}\right) \tag{12}$$

where C_3 is a constant and $\chi(\rho)$ is a function, both of which depend on laminate dimensions and material properties and are defined in the appendix. The first term in Eq. (12) is the strain energy in the absence of microcracks and the second term is the excess strain energy caused by the microcracks. Physically, $\chi(\rho)$ is proportional to the excess strain energy caused by two microcracks spaced by a dimensionless half spacing of ρ.

2.4 Total Sample Strain Energy

Now we consider a $[(S)/90_n]_s$ laminate with N microcrack intervals or N elements of damage whose dimensionless spacings and delamination lengths are characterized by $\vec{\rho} = (\rho_1, \rho_2, \ldots, \rho_N)$ and $\vec{\delta} = (\delta_1, \delta_2, \ldots, \delta_N)$. The total strain energy in such a sample is

$$\begin{aligned} U = \sum_{i=1}^{N} \left(U_{I+III}(\delta_i) + U_{II}(\rho_i, \delta_i)\right) = \left(\frac{\sigma_0^2}{2E_c} + \frac{t_1 \Delta\alpha^2 T^2}{C_1 B}\right)(L-D)BW \\ + \frac{\sigma_0^2}{2E_x^{(2)}} \frac{1+\lambda}{\lambda} DBW + C_3 t_1 (L-D)W \left(\frac{{E_x^{(1)}}^2}{E_c^2}\sigma_0^2 - \frac{\Delta\alpha^2 T^2}{C_1^2}\right) \frac{\sum_{i=1}^{N} \chi(\rho_i - \delta_i)}{\sum_{i=1}^{N}(\rho_i - \delta_i)} \end{aligned} \tag{13}$$

In deriving Eq. (13), we have used the total sample length L and the total delamination length D, given by

$$L = \sum_{i=1}^{N} 2t_1 \rho_i \qquad \text{and} \qquad D = \sum_{i=1}^{N} 2t_1 \delta_i \tag{14}$$

3. Modulus, Compliance, and Thermal Expansion Coefficient

The stresses and strain energy derived in the previous section can be used to find the effective modulus, compliance, and longitudinal thermal expansion coefficient. At the residual stress-free temperature, the total strain energy of a microcracked and delaminated laminate is

$$U = \frac{\sigma_0^2}{2E_{eff}} LBW \tag{15}$$

where E_{eff} is the effective longitudinal modulus of the sample. We take Eq. (15) as the definition of E_{eff} and equate it to the strain energy in Eq. (13) at the stress-free temperature ($T = 0$) to yield

$$\frac{1}{E_{eff}} = \frac{1}{E_c} + \frac{2t_1 {E_x^{(1)}}^2}{BE_c^2} \left(\frac{C_3(L-D)}{L} \frac{\sum \chi(\rho_i - \delta_i)}{\sum(\rho_i - \delta_i)} + \frac{C_1 D}{L}\right) \tag{16}$$

Multiplying both sides of Eq. (16) by $\frac{L}{BW}$ results in an expression for sample compliance:

$$C = \frac{L}{BE_{eff}W} = C_0 + \frac{2t_1 {E_x^{(1)}}^2}{B^2 W E_c^2} \left(C_3(L-D) \frac{\sum \chi(\rho_i - \delta_i)}{\sum(\rho_i - \delta_i)} + C_1 D\right) \tag{17}$$

where

$$C_0 = \frac{L}{BE_c W} \tag{18}$$

is the compliance of the undamaged laminate. By a principle of variational mechanics, Eq. (13) is an upper bound to the true strain energy; this fact implies that Eq. (16) defines a lower bound to the true modulus and that Eq. (17) defines an upper bound to the true compliance. Experimental evidence suggests that the bounds are tight [5].

We examine the limiting values of the compliance. In the limit of no delaminations, $D = 0$, Eq. (17) reduces to the results in Refs. [5,6,9,10]. In the limit of complete delamination, $D = L$, the sample compliance reduces to

$$C_\infty = \frac{1+\lambda}{\lambda} \frac{L}{BE_x^{(2)} W} \tag{19}$$

which is the compliance for a sample in which the $[90_n]$ sublaminate carries no load.

Using Eq. (17) to rewrite the total strain energy in terms of compliance, we quickly achieve

$$U = \left(\frac{\sigma_0^2}{2E_c} + \frac{t_1\Delta\alpha^2T^2}{C_1B}\right)LBW + (C-C_0)\frac{B^2W^2E_c^2}{2{E_x^{(1)}}^2}\left(\frac{{E_x^{(1)}}^2}{E_c^2}\sigma_0^2 - \frac{\Delta\alpha^2T^2}{C_1^2}\right) \tag{20}$$

Eq. (20) has the same form as the expression for strain energy in a laminate that has microcracks but has no delaminations [9,10]. Because the expression for compliance (Eq. (17)) depends on D, however, the strain energy in a microcracked and delaminated laminate will differ from the strain energy in a laminate that has microcracks only. In the limit of no delaminations ($D = 0$) the expression for compliance reduces to the expression for a laminate that has only microcracks and thus Eq. (20) is identical to the results in Refs. [9] and [10]. In the limit of complete delamination ($D = L$) the compliance becomes $C = C_\infty$ and the strain energy reduces to

$$U_\infty = \frac{\sigma_0^2}{2E_x^{(2)}}\frac{1+\lambda}{\lambda}LBW = \frac{{\sigma_{xx}^{(2)}}^2}{2E_x^{(2)}}2t_2LW \tag{21}$$

which is the total strain energy for the completely delaminated sample in which constant tensile stresses in the (S) sublaminate carry all the load transferred from the $[90_n]$ sublaminate. The limiting values for Eq. (20) are in accordance with expectation.

To get the longitudinal thermal expansion coefficient we need to calculate the total displacement of the uncracked 0° plies. Introducing the notation $u_i(P)$ as the total longitudinal displacement across all region i's under load P, the longitudinal thermal expansion coefficient of the microcracked and delaminated laminate is

$$\alpha_L = \frac{u_I(0) + u_{II}(0) + u_{III}(0)}{LT} = \frac{u(0)}{LT} \tag{22}$$

The zero-load displacements in regions I and III can be found by a simple integration of the strains in those regions:

$$u_I(0) + u_{III}(0) = \sum_{i=1}^{N}\int_0^{d_{1,i}+d_{2,i}} \varepsilon_{xx}(0)dx = \sum_{i=1}^{N}\int_0^{2\delta_i t_1} \alpha_x^{(2)}Tdx = \alpha_x^{(2)}DT \tag{23}$$

The displacement in region II for a crack interval of dimensionless half spacing $\rho - \delta$ can be derived from the results in Ref. [9] as

$$u_{II}(0) = (L-D)\left(\alpha_x^{(2)}T + \frac{\Delta\alpha T}{\lambda E_x^{(2)}C_1} - \frac{C_3\Delta\alpha T}{\lambda E_x^{(2)}C_1^2}\frac{\sum_{i=1}^N \chi(\rho_i-\delta_i)}{\sum_{i=1}^N(\rho_i-\delta_i)}\right) \tag{24}$$

Combining these results gives

$$\alpha_L = \alpha_x^{(2)} + \frac{\Delta\alpha}{\lambda E_x^{(2)}C_1} - \frac{D}{L}\frac{\Delta\alpha}{\lambda E_x^{(2)}C_1} - \left(\frac{L-D}{L}\right)\frac{C_3\Delta\alpha}{\lambda E_x^{(2)}C_1^2}\frac{\sum_{i=1}^N \chi(\rho_i-\delta_i)}{\sum_{i=1}^N(\rho_i-\delta_i)} \tag{25}$$

Substituting the expression for C_1 in the appendix, we can combine the first two terms to yield

$$\alpha_x^{(2)} + \frac{\Delta\alpha}{\lambda E_x^{(2)}C_1} = \frac{\lambda E_x^{(2)}\alpha_x^{(2)} + \alpha_x^{(1)}E_x^{(1)}}{\lambda E_x^{(2)} + E_x^{(1)}} = \alpha_L^0 \tag{26}$$

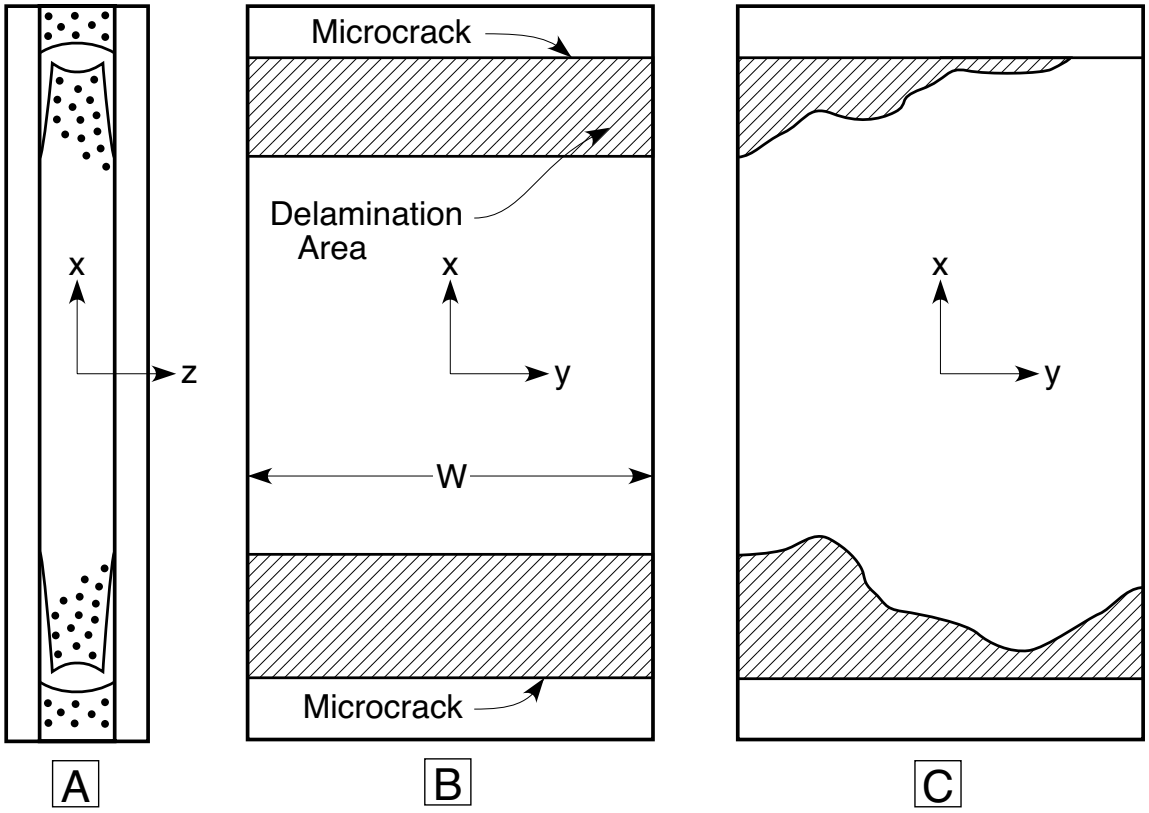

Figure 2: A. An edge view of a representative element of damage having microcracks and delaminations. B. A side view (sample width view) of through-the-width delaminations. The shaded areas indicate areas of delamination. C. A side view (sample width view) of arbitrarily shaped delamination fronts

where α_L^0 is the rule-of-mixtures longitudinal thermal expansion coefficient of the undamaged laminate. Using Eq. (17) we quickly achieve

$$\alpha_L = \alpha_L^0 - \frac{C - C_0}{C_0} \frac{\Delta\alpha}{C_1 E_x^{(1)}} \tag{27}$$

As with the expression for strain energy, Eq. (27) has the same form as the expression for longitudinal thermal expansion coefficient in a laminate that has microcracks but no delaminations [9,10]. Because the expression for compliance (Eq. (17)) depends on D, however, the thermal expansion coefficient of a microcracked and delaminated laminate will differ from that of a laminate that has only microcracks. Eq. (27) again has the appropriate limiting values. In the limit of no delaminations ($D = 0$) the expression for compliance reduces to the expression for a laminate that has only microcracks and Eq. (20) is identical to the results in Refs. [9] and [10]. In the limit of complete delamination ($D = L$) the compliance becomes $C = C_\infty$ and the thermal expansion coefficient reduces to $\alpha_L = \alpha_x^{(2)}$ which is as expected for the case that the (S) sublaminate is completely delaminated from the $[90_n]$ sublaminate.

4. Energy Release Rate for a Through-The-Width Delamination

The results of the two-dimensional stress analysis can be used to calculate the energy release rate for self-similar, through-the width delamination growth. The delamination growth process is shown in Fig. 2B. By definition the total energy release rate is

$$G_D = -\frac{\partial U}{\partial A}\bigg|_{const.u} = -\frac{1}{2W}\frac{\partial U}{\partial D}\bigg|_{const.u} \tag{28}$$

where A is total delamination area. For symmetric delamination growth $A = 2DW$. Because all partial derivatives are taken at constant displacement, only σ_0 and C in Eq. (20) are functions of D. We thus quickly achieve

$$\frac{\partial U}{\partial D}\bigg|_{const.u} = B^2W^2\left[C\sigma_0\frac{\partial \sigma_0}{\partial D}\bigg|_{const.u} + \left(\frac{\sigma_0^2}{2} - \frac{\Delta\alpha^2T^2E_c^2}{2C_1^2{E_x^{(1)}}^2}\right)\frac{\partial C}{\partial D}\right] \tag{29}$$

Using the relation between sample compliance, load, and displacement

$$CP = u(P) - u(0) = u(P) - \alpha_L LT \tag{30}$$

and realizing that α_L depends on D yield [10]:

$$\frac{\partial \sigma_0}{\partial D}\bigg|_{const.u} = \left(\frac{E_c\Delta\alpha T}{E_x^{(1)}C_1} - \sigma_0\right)\frac{1}{C}\frac{\partial C}{\partial D} \tag{31}$$

Substituting Eqs. (31) and (29) into Eq. (28) gives

$$G_D = \frac{B^2WE_c^2}{4{E_x^{(1)}}^2}\left(\frac{E_x^{(1)}}{E_c}\sigma_0 - \frac{\Delta\alpha T}{C_1}\right)^2\frac{\partial C}{\partial D} \tag{32}$$

Differentiating Eq. (17) and substituting the result into Eq. (32) lead to

$$G_D = C_3t_1\left(\frac{E_x^{(1)}}{E_c}\sigma_0 - \frac{\Delta\alpha T}{C_1}\right)^2 Y_D(\vec{\rho},\vec{\delta}) \tag{33}$$

where $Y_D(\vec{\rho},\vec{\delta})$ is a function of $\vec{\rho} = (\rho_1, \rho_2, \ldots, \rho_N)$ and $\vec{\delta} = (\delta_1, \delta_2, \ldots, \delta_N)$:

$$Y_D(\vec{\rho},\vec{\delta}) = \frac{1}{2}\left((L-D)\frac{\partial}{\partial D}\frac{\sum_{i=1}^N \chi(\rho_i - \delta_i)}{\sum_{i=1}^N(\rho_i - \delta_i)} - \frac{\sum_{i=1}^N \chi(\rho_i - \delta_i)}{\sum_{i=1}^N(\rho_i - \delta_i)} + \frac{C_1}{C_3}\right) \tag{34}$$

We achieve a dramatic simplification by considering a differential amount of delamination growth at one of the through-the-width delamination fronts. Assuming delamination growth occurs in the k^{th} microcrack interval, the differential delamination growth is $dD = 2t_1d\delta_k$. The $Y_D(\vec{\rho},\vec{\delta})$ function for this delamination growth is

$$Y_D(\vec{\rho},\vec{\delta}) = \frac{C_1}{2C_3} - \frac{\chi'(\rho_k - \delta_k)}{2} \tag{35}$$

The function $\chi'(\rho)$ is defined in the appendix. We achieve a slightly more pleasing result by noting that

$$\lim_{\rho\to 0}\chi'(\rho) = \chi'(0) = \frac{C_1}{C_3} \tag{36}$$

The final expression for the total energy release rate for self-similar, through-the-width delamination growth is

$$G_D = C_3 t_1 \left(\frac{E_x^{(1)}}{E_c}\sigma_0 - \frac{\Delta\alpha T}{C_1} \right)^2 \frac{\chi'(0) - \chi'(\rho_k - \delta_k)}{2} \tag{37}$$

Note that Eq. (37) depends only on the magnitude of $\rho_k - \delta_k$ or the separation between the tips of two growing delaminations. It is thus possible for the energy release rate for a long delamination to be the same as that of a short delamination. This equality will occur when the microcrack interval for the long delamination is sufficiently long such that the values of $\rho_k - \delta_k$ are the same for each delamination. We are often concerned with the energy release rate for initiation of delamination when $\delta_k = 0$. For initiation, the energy release rate depends only on the size of the microcrack interval, ρ_k.

5. Quasi Three-Dimensional Analysis

Experimental observations of microcrack induced delaminations suggest that delamination growth is not necessarily self-similar and through-the-width [1,4]. A typical delamination begins at an edge where its initiation is probably driven by free-edge interlaminar normal stresses [15,17]. After initiation it may propagate in either the x direction (parallel to the applied load), the y direction (perpendicular to the applied load), or at some angle β with respect to the applied load, depending on which direction has the maximum energy release rate [20]. The general propagation of a non-through-the-width delamination is a three-dimensional problem. We propose a quasi-three-dimensional model using lumped springs. A lumped spring model ignores free-edge stresses and we therefore focus on delamination growth interior to the laminate. Interior delamination is defined as the growth of an initial edge delamination after propagating a few ply depths from the edge [15], or as the growth of a delamination that initiates interior to the laminate.

Consider an arbitrarily shaped delamination front within microcrack interval k (see Fig. 2C). We divide this interval into n parallel elements of width $W^{(j)}$ ($j = 1, 2, \ldots n$) having dimensionless delamination length $\delta_k^{(j)}$ derived from delamination profile at the element position (see Fig. 3A). Each element has the same length $L^{(j)} = 2\rho_k t_1$, but individual delamination length $D^{(j)} = 2\delta_k^{(j)} t_1$, compliance $C^{(j)}$, and thermal expansion coefficient $\alpha_L^{(j)}$. The compliance and thermal expansion coefficient of each element are given by the two-dimensional results in Eqs. (17) and (27) with sample dimensions replaced by element dimensions. During delamination growth in interval k, the remaining microcrack intervals experience no delamination growth and thus can be lumped into a single element labeled element 0. Element 0 is has length $L^{(0)} = L - 2\rho_k t_1$, delamination length

$$D^{(0)} = D - 2t_1 \frac{\sum_{j=1}^{n} \delta_k^{(j)} W^{(j)}}{\sum_{j=1}^{n} W^{(j)}},$$

compliance $C^{(0)}$, and thermal expansion coefficient $\alpha_L^{(0)}$. As shown in Fig. 3B, the quasi-three-dimensional model replaces each element by a linear spring. Element 0 is connected in series with the n elements in microcrack interval k, which are connected in parallel. The parallel arrangement of the elements in microcrack interval k provides a uniform strain boundary condition at the microcrack surfaces that prevents displacement discontinuity along the microcrack.

A small amount of delamination growth can be modeled as an increase in $\delta_k^{(j)}$ in element j. Without loss of generality we lump the remaining elements into a single element to construct a three element model (see

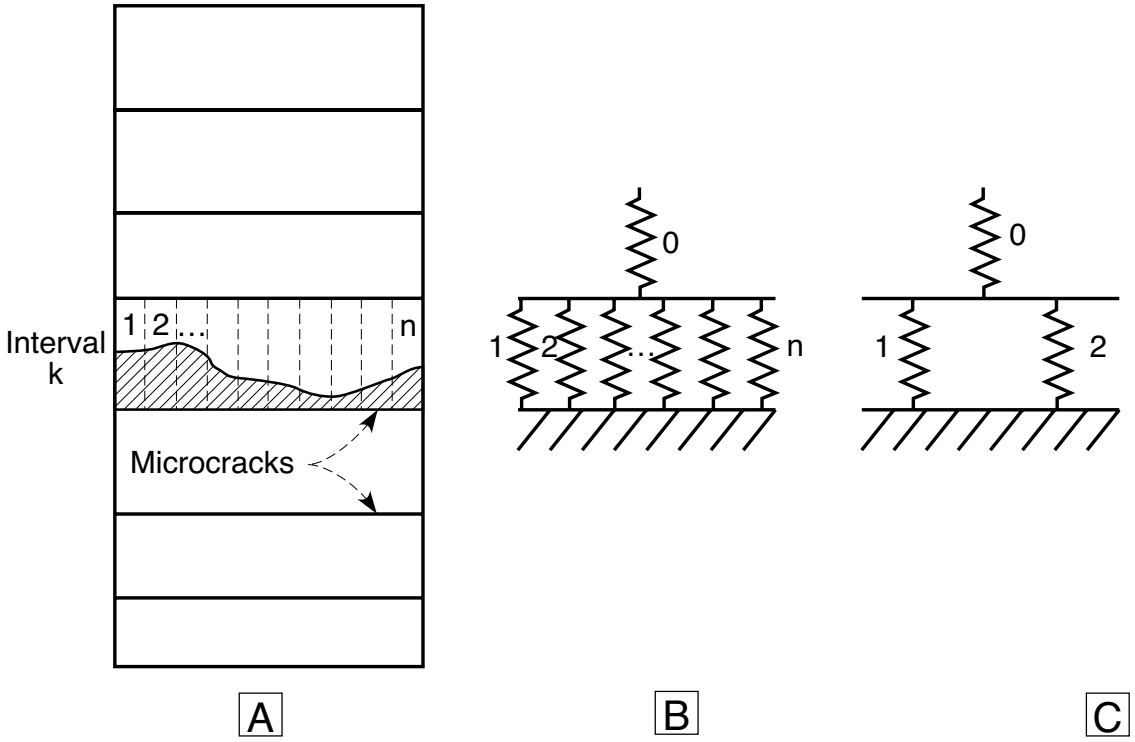

Figure 3: A. A side view of a laminate having microcracks and an arbitrarily shaped delamination front in microcrack interval k. B. Microcrack interval k is divided into n springs loaded in parallel; the remainder of the sample is lumped into spring 0. C. Spring 1 is the element that experiences delamination growth; the remaining elements in microcrack interval k are lumped into spring 2.

Fig. 3C). Element 0 is defined above. Element 1 is the element j where delamination growth occurs. It has a width $W^{(1)}$ and a delamination changing from $2t_1\delta_k^{(1)}$ to $2t_1\delta_k^{(1)} + dD$. Element 2 has an effective compliance and a thermal expansion coefficient characteristic of the remaining elements. Its width is $W - W^{(1)}$.

For a differential amount of crack growth dD in element 1, the differential delamination fracture area is $dA = 2W^{(1)}dD$ and the energy release rate is

$$G_D = -\frac{1}{2W^{(1)}}\left(\left.\frac{\partial U^{(0)}}{\partial D}\right|_{const.u} + \left.\frac{\partial U^{(1)}}{\partial D}\right|_{const.u} + \left.\frac{\partial U^{(2)}}{\partial D}\right|_{const.u}\right) \tag{38}$$

where $U^{(i)}$ is the strain energy of element i. The derivative of $U^{(i)}$ is given by Eq. (29) with element properties and element stress, $\sigma^{(j)}$, replacing sample properties and sample stress, σ_0. Realizing that $\sigma^{(0)} = \sigma_0$ and that $\frac{\partial C^{(0)}}{\partial D} = \frac{\partial C^{(2)}}{\partial D} = 0$ we have

$$\begin{aligned} G_D = -\frac{B^2}{2W^{(1)}}\Bigg[& W^2 C^{(0)}\sigma_0 \left.\frac{\partial \sigma_0}{\partial D}\right|_{const.u} + \left(W - W^{(1)}\right)^2 C^{(2)}\sigma^{(2)} \left.\frac{\partial \sigma^{(2)}}{\partial D}\right|_{const.u} \\ & + {W^{(1)}}^2 \left(C^{(1)}\sigma^{(1)} \left.\frac{\partial \sigma^{(1)}}{\partial D}\right|_{const.u} + \frac{{\sigma^{(1)}}^2}{2}\frac{\partial C^{(1)}}{\partial D} - \frac{\Delta\alpha^2 T^2 E_c^2}{2C_1^2 {E_x^{(1)}}^2}\frac{\partial C^{(1)}}{\partial D}\right)\Bigg] \end{aligned} \tag{39}$$

Equation (39) has five unknowns — $\sigma^{(1)}$, $\sigma^{(2)}$, $\frac{\partial \sigma^{(1)}}{\partial D}$, $\frac{\partial \sigma^{(2)}}{\partial D}$, and $\frac{\partial \sigma_0}{\partial D}$. We need five equations to determine these unknowns. Force balance has the form

$$W^{(1)}\sigma^{(1)} + \left(W - W^{(1)}\right)\sigma^{(2)} = W\sigma_0 \tag{40}$$

Differentiating Eq. (40) gives

$$W^{(1)}\frac{\partial\sigma^{(1)}}{\partial D}+\left(W-W^{(1)}\right)\frac{\partial\sigma^{(2)}}{\partial D}=W\frac{\partial\sigma_0}{\partial D} \tag{41}$$

The constant displacement boundary condition for the entire sample leads to

$$BWC^{(0)}\sigma_0+\alpha_L^{(0)}\left(L-L^{(1)}\right)T+B\left(W-W^{(1)}\right)C^{(2)}\sigma^{(2)}+\alpha_L^{(2)}L^{(1)}T=constant \tag{42}$$

which is differentiated to yield

$$WC^{(0)}\frac{\partial\sigma_0}{\partial D}+\left(W-W^{(1)}\right)C^{(2)}\frac{\partial\sigma^{(2)}}{\partial D}=0 \tag{43}$$

The equality of displacements of elements 1 and 2 gives

$$BW^{(1)}C^{(1)}\sigma^{(1)}+\alpha_L^{(1)}L^{(1)}T=B\left(W-W^{(1)}\right)C^{(2)}\sigma^{(2)}+\alpha_L^{(2)}L^{(1)}T \tag{44}$$

Differentiating Eq. (44) and using Eq. (27) result in

$$B\left(W-W^{(1)}\right)C^{(2)}\frac{\partial\sigma^{(2)}}{\partial D}=BW^{(1)}C^{(1)}\frac{\partial\sigma^{(1)}}{\partial D}+\left(BW^{(1)}\sigma^{(1)}\ -\frac{\Delta\alpha L^{(1)}T}{C_1C_0^{(1)}E_x^{(1)}}\right)\frac{\partial C^{(1)}}{\partial D} \tag{45}$$

Using Eqs. (40), (41), (43), (44), and (45) and eliminating all except the stress in element 1 ($\sigma^{(1)}$), the energy release rate in Eq. (39) reduces to

$$G_D=C_3t_1\left(\frac{E_x^{(1)}}{E_c}\sigma^{(1)}-\frac{\Delta\alpha T}{C_1}\right)^2\frac{\chi'(0)-\chi'(\rho_k-\delta_k^{(1)})}{2} \tag{46}$$

Equation (46) is identical to the two-dimensional result in Eq. (37) except that it uses delamination length, $\delta_k^{(1)}$, and stress, $\sigma^{(1)}$, at the point of delamination growth. From Eqs. (40) and (44) we obtain

$$\sigma^{(1)}=\frac{\frac{\sigma_0W}{\left(W-W^{(1)}\right)E^{(2)}}+\left(\alpha_L^{(2)}-\alpha_L^{(1)}\right)T}{\frac{1}{E^{(1)}}+\frac{W^{(1)}}{\left(W-W^{(1)}\right)E^{(2)}}} \tag{47}$$

We can define the energy release rate at a point along an arbitrarily shaped delamination front by passing to the limit as $W^{(1)}\to 0$. The result is

$$G_D=C_3t_1\left(\frac{E_x^{(1)}E^{(1)}}{E_c}\left(\frac{\sigma_0}{E^{(2)}}+\left(\alpha_L^{(2)}-\alpha_L^{(1)}\right)T\right)-\frac{\Delta\alpha T}{C_1}\right)^2\frac{\chi'(0)-\chi'(\rho_k-\delta_k^{(1)})}{2} \tag{48}$$

G_D is a function of elements 1 and 2 only, which in turn depend only on the size of microcrack interval k and on the shape of the delamination front. When the delamination front is uniform, $E^{(1)}=E^{(2)}$, $\alpha_L^{(1)}=\alpha_L^{(2)}$, $\delta_k^{(1)}=\delta_k$, and the energy release rate reduces to the two-dimensional result in Eq. (37).

Lastly, we need to calculate $E^{(1)}$, $E^{(2)}$, $\alpha_L^{(1)}$, and $\alpha_L^{(2)}$. When the width of element 1 approaches zero ($W^{(1)}\to 0$), the width of element 2 approaches W. Recall from Fig. 3B that element 2 is a conglomerate of $n-1$ parallel springs. A simple calculation for $n-1$ parallel springs taken in the limit as $n\to\infty$ results in

$$E^{(2)}=\frac{1}{W}\int_0^W E\big(\delta_k(y)\big)dy \tag{49}$$

$$\alpha_L^{(2)}=\frac{\int_0^W\alpha_L\big(\delta_k(y)\big)E\big(\delta_k(y)\big)dy}{\int_0^W E\big(\delta_k(y)\big)dy} \tag{50}$$

Table I: Typical mechanical properties for various sublaminates of a carbon fiber/epoxy laminate. The properties of the [±45] sublaminate were calculated from the [0] and [90] laminate properties using laminated plate theory

Property	[0]	[90]	[±45]
E_x (MPa)	128000	7200	12453
E_z (MPa)	7200	7200	12453
G_{xz} (MPa)	4000	2400	13176
ν_{xz}	0.3	0.5	0.557
α_x(ppm/°C)	-0.09	28.8	6.55
α_z(ppm/°C)	28.8	28.8	6.55
Ply thickness (mm)	0.14	0.14	0.14

where $\delta_k(y)$ describes the delamination profile and $E\big(\delta_k(y)\big)$ and $\alpha_L\big(\delta_k(y)\big)$ are given by a two-dimensional analysis of a single microcrack interval (*c. f.* Eqs. (16) and (25)):

$$\frac{1}{E\big(\delta_k(y)\big)} = \frac{1}{E_c} + \frac{2C_3t_1{E_x^{(1)}}^2}{\rho_k B E_c^2}\left(\chi(\rho_k-\delta_k(y)) + \frac{C_1\delta_k(y)}{C_3}\right) \tag{51}$$

$$\alpha_L\big(\delta_k(y)\big) = \alpha_L^0 - \frac{2C_3t_1E_x^{(1)}}{\rho_k B E_c C_1}\left(\chi(\rho_k-\delta_k(y)) + \frac{C_1\delta_k(y)}{C_3}\right) \tag{52}$$

In element 1, $E^{(1)}$ and $\alpha_L^{(1)}$ also come from Eqs. (51) and (52) by letting $E^{(1)} = E(\delta_k^{(1)})$ and $\alpha_L^{(1)} = \alpha(\delta_k^{(1)})$.

6. Results and Discussion

The variational analysis for the through-the-width delamination is the foundation of this study. It is an extension of the variational analysis for microcracking in cross-ply laminates [9,10]. Because of the assumption of constant x-axis tensile stress within sublaminates, the delaminated portions of the $[90_{2n}]_T$ sublaminate takes no load. An advance of delamination, therefore, can be interpreted as a move of the microcrack from which the delamination initiates. This interpretation can be demonstrated by Eq. (37) in which the excess strain energy function, $\chi(\rho)$, appears in the form of a derivative. In the corresponding equation for energy release rate due to the formation of new microcracks [9,10], $\chi(\rho)$ appears as a step function or as the difference between the final and initial total $\chi(\rho)$ functions (see below). In extending the microcracking analysis to include delamination, the use of variational mechanics assures the best analytical results for stress state and strain energy release rate. A better analytical result could only be obtained by relaxing the only assumption about $\sigma_{xx}^{(i)}$. Relaxing this assumption would be difficult or impossible in terms of achieving closed-form solutions. The remainder of this section considers predictions derived from the delamination energy release rate analysis.

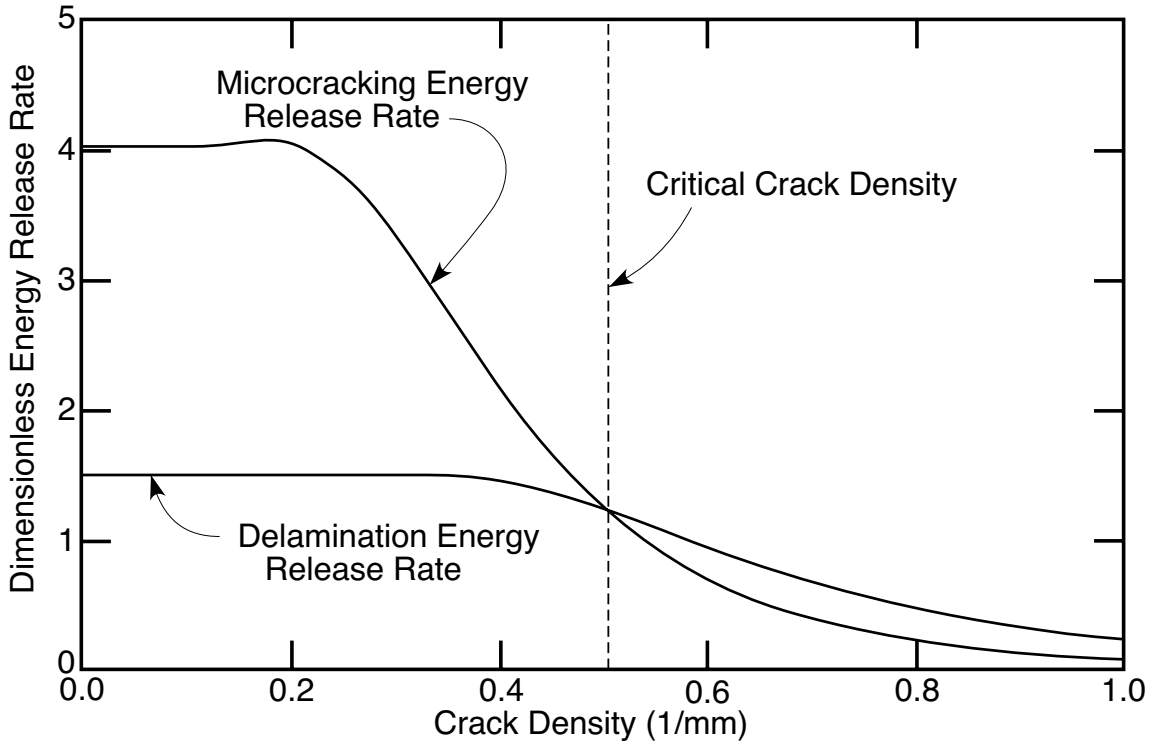

Figure 4: Dimensionless energy release rates for initiation of delamination and for continued microcracking as functions of microcrack density. The critical crack density for delamination is defined by the crack density where the two curves cross.

6.1. Delamination Initiation

Our interest is in laminates of type $[(S)/90_n]_s$ in which the initial form of failure is microcracking of the 90° plies. Once the first microcrack has formed, the question is whether the next form of damage will be another microcrack or will be the initiation of a delamination induced by an existing microcrack. We seek to answer this question by examining which form of damage tends to release more strain energy. The energy release rate for initiation of a delamination in microcrack interval k is given by Eq. (37) with $\delta_k = 0$:

$$G_D = C_3 t_1 \left(\frac{E_x^{(1)}}{E_c} \sigma_0 - \frac{\Delta\alpha T}{C_1} \right)^2 \frac{\chi'(0) - \chi'(\rho_k)}{2} \tag{53}$$

From Refs. [9] and [10], the energy release rate for the formation of a microcrack is

$$G_m = C_3 t_1 \left(\frac{E_x^{(1)}}{E_c} \sigma_0 - \frac{\Delta\alpha T}{C_1} \right)^2 \big(2\chi(\rho_k/2) - \chi(\rho_k) \big) \tag{54}$$

These energy release rates are maximized for damage in the largest crack interval. For a sample of N microcrack intervals, ρ_k is thus the largest among $(\rho_1, \rho_2, \ldots, \rho_N)$.

We assume that fracture is controlled by a critical total energy release rate. Delamination will occur if G_D exceeds G_{Dc} — the critical energy release rate for delamination. Microcracking will occur if G_m exceeds G_{mc} — the critical energy release rate for microcracking. Because both delamination and microcracking are crack growth through the matrix or along the fiber/matrix interface, we further assume that $G_{Dc} = G_{mc}$.

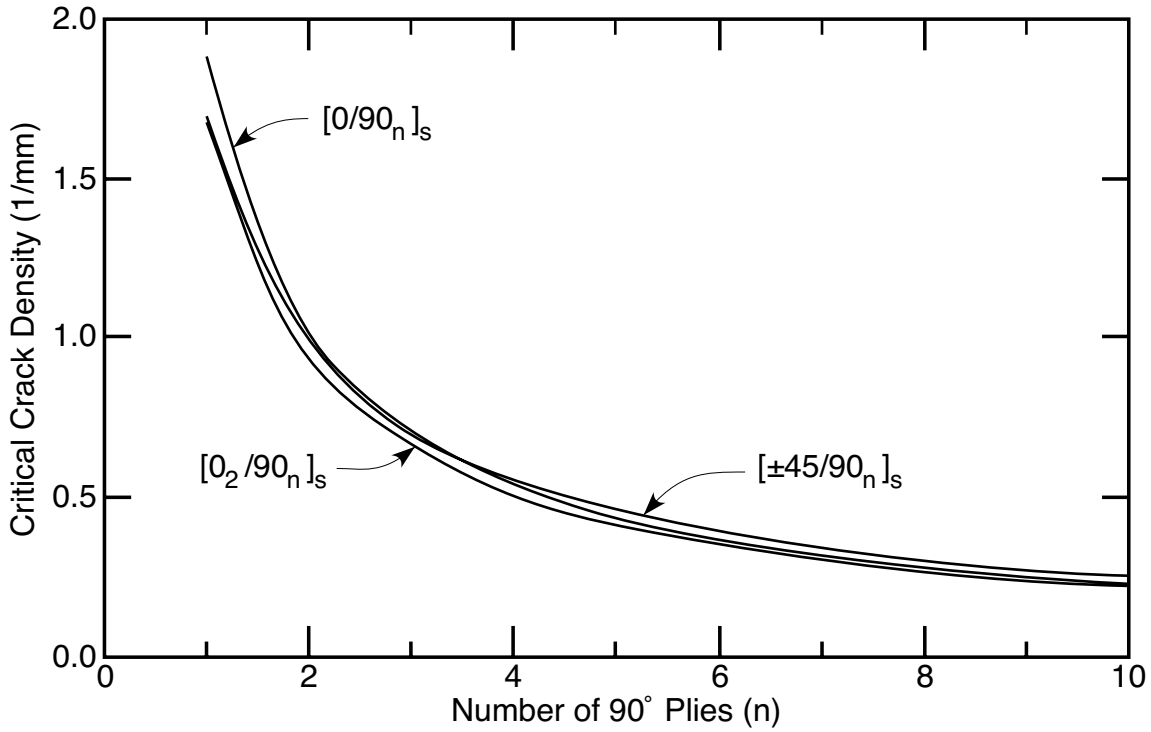

Figure 5: The critical crack densities for delamination as functions of the number of 90° plies in half of the symmetric laminate. The three curves are for different (S) sublaminates supporting the 90° plies.

Under these simplifying assumptions, the consequences of which will be discussed later, the expected failure mode can be predicted by plotting dimensionless energy release rates. Removing the common prefactors in Eqs. (53) and (54), we obtain dimensionless energy release rates for delamination, g_D, and for microcracking, g_m as

$$g_D = \frac{\chi'(0) - \chi'(\rho_k)}{2} \qquad \text{and} \qquad g_m = 2\chi(\rho_k/2) - \chi(\rho_k) \tag{55}$$

In Fig. 4 g_D and g_m are plotted as a function of crack density $\left(\frac{1}{2\rho_k t_1}\right)$ for a $[0_2/90_4]_s$ carbon fiber/epoxy laminate. The material properties used in the calculation are given in Table I.

Fig. 4 shows that at low crack densities, microcracking is the preferred mode of failure. At some critical crack density (0.51 cracks/mm in Fig. 4), however, the energy release rate for a through-the-width delamination surpasses the energy release rate for microcracking and delaminations will be expected to initiate at the microcrack tips. Once delaminations initiate, microcracking will cease and the delaminations will continue to grow. The critical crack density for delamination depends on the laminate structure. Figure 5 shows that critical crack densities as a function of the number of 90° plies for $[0/90_n]_s$, $[0_2/90_n]_s$, and $[\pm 45/90_n]_s$ laminates. In agreement with experimental observations [1,4], the more 90° plies, the lower the critical crack density for delamination. The critical crack density is virtually independent of the sublaminate (S) supporting the 90° plies. Although sublaminate (S) has little effect on critical crack density, it has a significant effect on the load at which the critical crack density is reached. Experimental observations [10] show that the stiffer the sublaminate (S), the higher the load required to reach a given crack density.

We previously assumed that fracture is controlled by a critical total energy release rate. Delamination and microcracking, however, may have significant mixed-mode character which makes it important to define

failure using a fracture surface. In mixed mode loading, fracture occurs when the combination of mode I, mode II, and mode III energy release rates satisfies some critical value

$$f_{cr} = f\left(G_I, G_{II}, G_{III}\right) \tag{56}$$

where $f\left(G_I, G_{II}, G_{III}\right)$ defines a fracture surface [19]. If, however, our interest is in failure at constant proportions of G_I, G_{II}, and G_{III} (*e.g.* p_I, p_{II}, p_{III}), the distinction between total energy release rate and a fracture surface is unimportant. Either approach will give the same answer because

$$f_{cr} = f\left(p_I G, p_{II} G, p_{III} G\right) \tag{57}$$

will be a function only of total G. In Fig. 4, we have considered delamination and microcracking as functions of microcrack interval size. We expect that microcrack interval size has little effect on the proportions of G_I, G_{II}, and G_{III} for these failure modes and thus conclude that predictions based on total energy release rate are valid. This expectation can be supported by finite element analysis which show that microcracking is mostly mode I and that delamination is mostly mode II.

We have further assumed that $G_{Dc} = G_{mc}$. Although both delamination and microcracking are types of matrix cracking, they are comprised of different proportions of G_I, G_{II}, and G_{III}. The disparate mixed-mode characters probably lead to $G_{Dc} \neq G_{mc}$. Fortunately, the conclusions drawn from Fig. 4 are easily generalized for $G_{Dc} \neq G_{mc}$. We merely need to normalize the dimensionless energy release rates by dividing them by the critical energy release rates. The trends of g_m and g_D will remain the same but one of them (*e.g.* g_m) will move up or down relative to the other, depending on $G_{mc} < G_{Dc}$ or $G_{mc} > G_{Dc}$. Consequently the critical crack density will increase (for $G_{mc} < G_{Dc}$) or decrease (for $G_{mc} > G_{Dc}$).

6.2. Delamination Propagation

At the critical crack density for delamination, we expect delaminations to initiate. We next plot the energy release rate as the delamination grows within a microcrack interval. Figure 6A shows the energy release rate for growth of a delamination in a 2 mm microcrack interval in a $[0_2/90_4]_s$ carbon fiber/epoxy laminate which corresponds to the interval size at the critical crack density in Fig. 4. Figure 6B shows the energy release rate for growth in a relatively large 10 mm microcrack interval. We include this plot to facilitate comparison to previous results which have exclusively been related to the delamination from isolated microcracks [13–17]. The energy release rates in Figs. 6A and 6B were calculated using $\sigma_0 = 200$ MPa and $T = 0$. The residual stress term was set to zero to facilitate comparison to previous results for which residual stresses have been ignored [13–17]. The straight lines in Figs. 6A and 6B are plots of O'Brien's "simple" analytical energy release rate that ignores the neighboring microcrack effect [13,14]. In the nomenclature of this paper the simple analytical result is

$$G_D = \frac{\sigma_0^2 B^2}{4}\left(\frac{1}{2t_2 E_x^{(2)}} - \frac{1}{BE_c}\right) \tag{58}$$

Eq. (58) has been shown to be in reasonable agreement with three-dimensional finite element analysis [15].

Beginning with Fig. 6B, the energy release rate remains constant as the delamination grows within a large microcrack interval until it eventually approaches the neighboring microcrack, at which point it

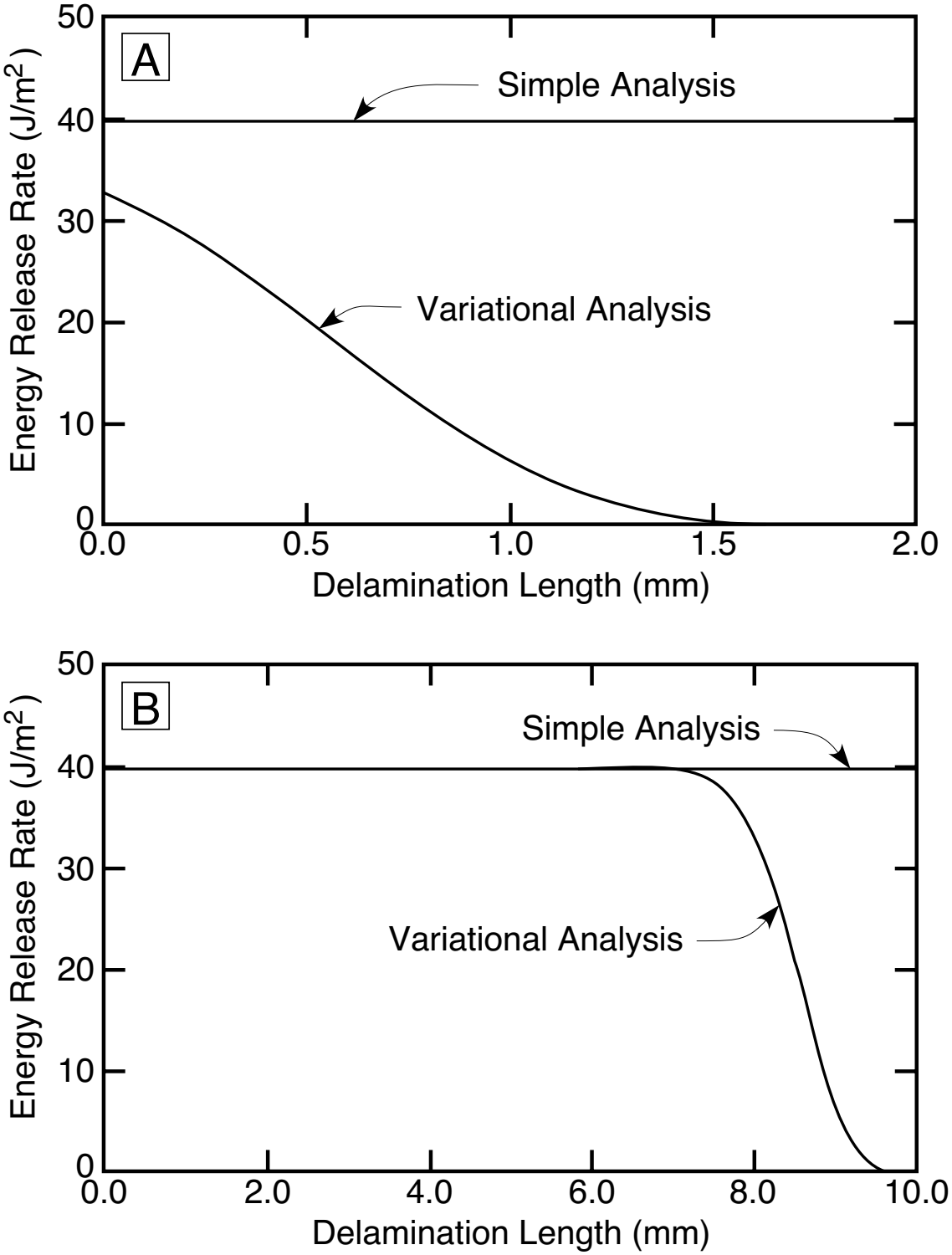

Figure 6: The energy release rate for delamination as a function of delamination length for a through-the-width delamination. A. Delamination growth in a small (2 mm) microcrack interval typical of those at crack densities higher than the critical crack density for delamination. B. Delamination growth in a large (10 mm) microcrack interval

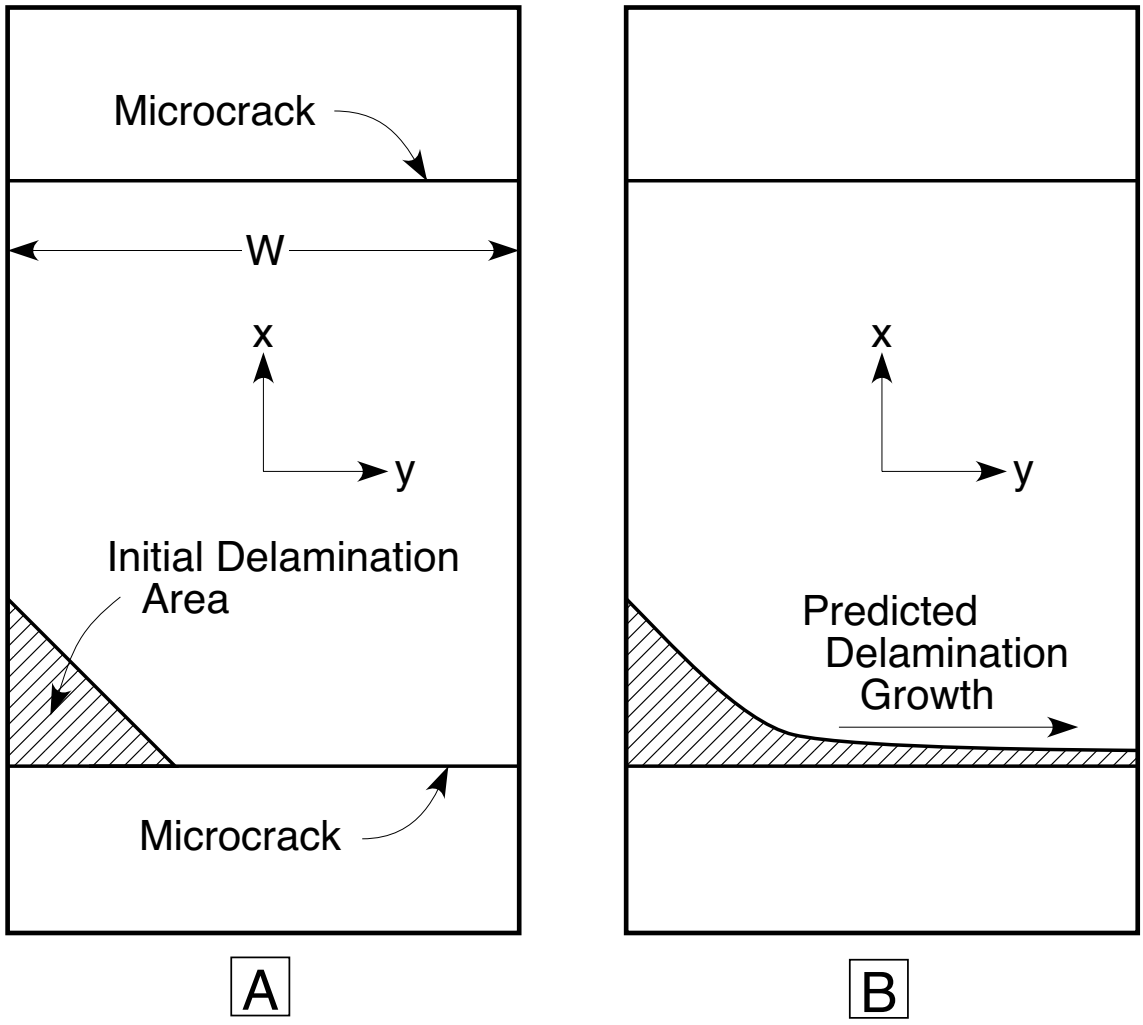

Figure 7: A schematic view of the predicted growth of a delamination emanating from a microcrack tip. A. An initial delamination growth is assumed to have a 45° crack front. B. If a 45° delamination front develops, it would be predicted to grow by extending along the microcrack tip or across the sample width.

rapidly decreases to zero. The constant portion predicted by the variational mechanics analysis is in excellent agreement with the simple analytical result. Taking the limit as $\rho \to \infty$, which gives $\chi'(\rho - \delta_k) = 0$, and setting $T = 0$, Eq. (37) reduces exactly to Eq. (58). In other words, the simple analytical result is a special case of Eq. (37). It applies to delamination growth from an isolated microcrack in the absence of residual thermal stresses. The variational mechanics analysis additionally accounts for residual thermal stresses and for the effect of encroaching on a neighboring microcrack.

Because delamination is not expected to initiate until the microcrack density has exceeded the critical crack density for delamination, the analysis of delamination from isolated microcracks is not the most relevant one. The more important problem is delamination growth in small microcrack intervals. A typical result in Fig. 6A shows that the energy release rate monotonically decreases as the delamination grows. The decreasing energy release rate and the lack of agreement with the simple analytical result are both consequences of the proximity of the neighboring microcrack.

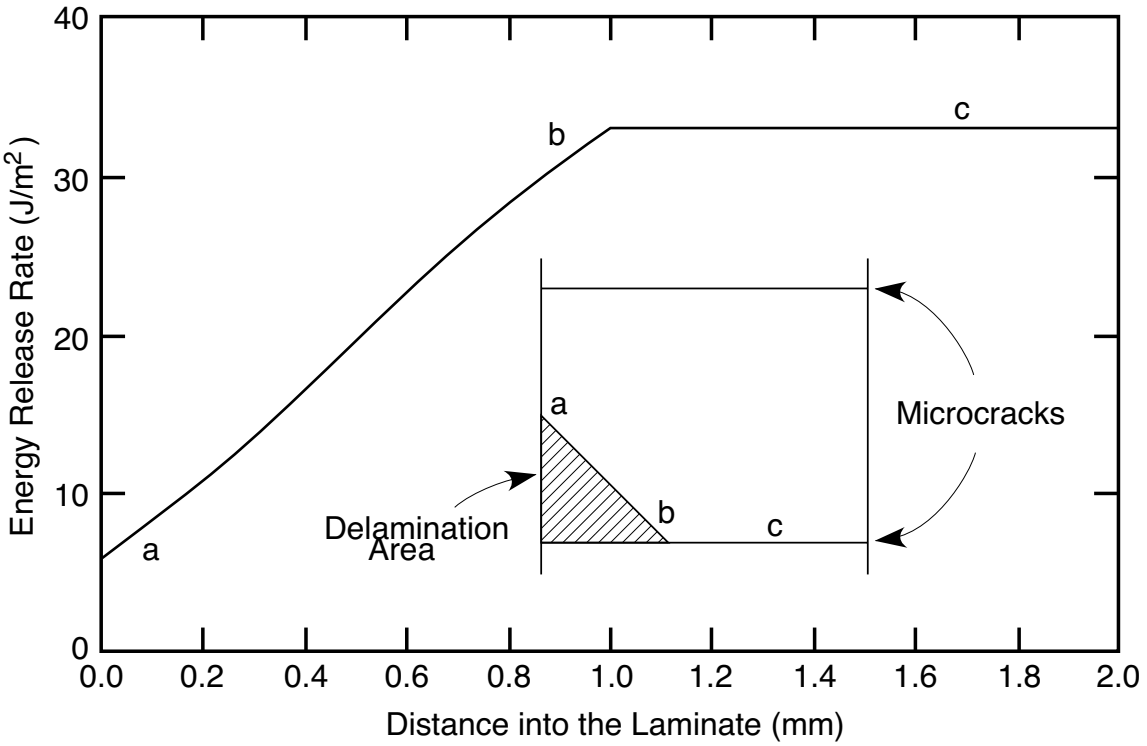

Figure 8: The energy release rate for delamination as a function of position along a 45° crack front. The assumed delamination extends 1 mm into a 2 mm microcrack interval. The letters a, b, and c show a position along the crack front and the corresponding position on the energy release rate plot.

6.3. Quasi-Three-Dimensional Model Results

We next apply the quasi-three-dimensional model to the analysis of a non-through-the-width delamination growth. Experimental observations [1,4] suggest that delaminations initiate at a free-edge with an angled crack front (see Fig. 7A). In Fig. 8 we use Eq. (48) to plot the energy release rate as a function of position along an angled delamination. The sample calculation is for a 12.7 mm wide $[0_2/90_4]_s$ carbon fiber/epoxy laminate with a 45° crack front that has grown 1 mm into a microcrack interval in which the microcracks are 2 mm apart. The energy release rate has its minimum at the free-edge, where $\delta_k(y)$ is the largest, and monotonically increases along the crack front as $\delta_k(y)$ monotonically decreases. When $\delta_k(y)$ becomes zero the energy release rate reaches a maximum and constant value. Assuming that delamination growth occurs at locations of maximum G_D, the quasi-three-dimensional model implies that delamination growth will proceed from regions of zero or minimum $\delta_k(y)$. As illustrated in Fig. 7B, we expect delamination growth to proceed along the microcrack tip where $\delta_k(y) = 0$. This form of crack growth will be preferred over self-similar propagation of the angled crack front. The predicted crack growth in Fig. 7B is in qualitative agreement with experimental observations in Refs. [1] and [4].

Two qualifications need to be placed on the predictions of the quasi-three-dimensional model. First, the tendency towards delamination growth from the region of minimum $\delta_k(y)$ is strong only for the small microcrack intervals typical for those beyond the critical crack density for delamination. In relatively large microcrack intervals, the energy release rate remains constant over a wide range of $\delta_k(y)$ and consequently

there will be no dominant delamination growth direction. Second, the quasi-three dimensional model can not account for free-edge interlaminar stresses. Three-dimensional finite element analysis shows that the free-edge stresses increase the loading for mode I fracture near the edge [15]. The increased mode I component may be responsible for the initiation of the delamination and for the initial observation of angled crack fronts. Once delamination growth has proceeded a few ply depths, the quasi-three-dimensional analysis in this paper will provide adequate predictions.

6.4. Assessment of Accuracy

Finally, we examine expected accuracy of the variational mechanics analysis. The only approximation made in the analysis is that within the ply groups, $\sigma_{xx}^{(i)}$ are functions of x but independent of z. This approximation is most severe near the microcrack tips and consequently results in expected stress singularities being ignored. Our fracture analysis, however, is not based on crack tip stress state, but rather on global strain energy. Despite missing stress singularities, we claim the global strain energy in Eq. (13) is sufficiently accurate. There are three pieces of evidence to support this claim. First, all limiting values are correct; *i.e.* the strain energy, modulus, and thermal expansion coefficient all give the correct results in the limit of zero or complete delamination. Second, there are precedents for laminate energy release rate analyses that ignore stress singularities to give accurate results. Two examples are double cantilever beam delamination [21] and edge delamination [22]. We suggest that the approximation used in this paper is the tensile loading analog of the standard beam theory approximation. This suggestion implies that our results have an accuracy similar to that of beam theories for delamination. The third piece of evidence supporting sufficient accuracy is that all predictions are at least qualitatively in agreement with experimental observations. A more quantitative test of the analysis will require more detailed experiment results.

An alternative delamination analysis could be developed using one-dimensional shear-lag methods. Such one-dimensional models are popular for quantifying the effect of microcracks (*e.g.* Refs. [23–30]). Like the variational analysis, the one-dimensional shear-lag models also assume that $\sigma_{xx}^{(i)}$ is a function of x only. Unlike the variational analysis, however, the one-dimensional models make additional assumptions that remove the z coordinate from the analysis and leave the transverse normal stresses undefined. Recent experiments on microcracking have shown that the extra assumptions render the one-dimensional stress analyses severely inadequate for interpreting microcracking experiments [31]. In contrast, the variational analysis can satisfactorily explain a wide body of microcracking results [31]. We claim that the requirements of an approximate stress analysis for delamination are even more severe. While the validity of the variational approach to delamination remains to be experimentally verified, the likelihood that a one-dimensional shear-lag analysis will provide any useful results is very low.

7. Conclusions

When the sublaminate (S) in a $[(S)/90_n]_s$ laminate is sufficiently stiff and n is not too small, the initial form of damage will be microcracking in the 90° plies. The variational mechanics analysis for delamination initiating at microcrack tips predicts that microcracking will continue until the microcrack density reaches some critical crack density for delamination. This critical crack density is determined by material properties, laminate

structure, the fracture toughness for delamination, G_{Dc}, and the fracture toughness for microcracking, G_{mc}. The more 90° plies, the lower will be the critical crack density for delaminations. The absolute critical crack density is nearly independent of the properties of the supporting sublaminate (S).

Experimental observations [1,4] show that delaminations initiate at the free-edge. Three-dimensional finite element analysis [15] indicates that this initiation is driven by an increased mode I loading near the free-edge. The current variational analysis is two-dimensional and therefore does not account for interlaminar normal stresses induced by a free edge. It therefore makes no prediction about delamination growth near the edge. Once the delamination has propagated a few ply depths into the sample, however, the quasi-three-dimensional analysis predicts that for typical microcrack intervals it will proceed along the microcrack tip and not by self-similar crack growth on an angled crack front. In brief, the dominant delamination growth is expected to be normal to the applied load or across the sample width.

The analysis and predictions in this paper are for laminates with interior 90° plies. Experimental observations show that the microcracking and delamination properties of laminates with outer-ply 90° plies (e.g. $[90_n/(S)]_s$) are much different from those with interior 90° plies [32]. We recently completed a variational mechanics analysis for microcracking in $[90_n/0_n]_s$ laminates [32], which are observed and predicted to form staggered microcracks. The asymmetry of the characteristic damage state leads to a bending effect that adds to the mode I type initiation of delaminations induced by microcracks [32]. In a future publication we will extend the analysis of Ref. [32] to account for delaminations emanating from staggered microcracks.

Appendix A

The stresses in a $[(S)/90_n]_s$ laminate are expressed in terms of an unknown function $\psi(x)$ in Eq. (1). By the principle of minimum complementary energy, the function $\psi(x)$ that minimizes the complementary energy will provide the best approximation to the stress state. Including thermal stresses, the complementary energy is minimized by minimizing

$$\Gamma = \frac{1}{2}\int_V \vec{\sigma}\cdot\mathbf{K}\vec{\sigma}\,dV + \int_V \vec{\sigma}\cdot\vec{\alpha}T\,dV - \int_{S_1}\vec{\sigma}\cdot\hat{u}\,dS \qquad (A1)$$

where $\vec{\sigma}$ is the stress tensor, $\mathbf{K}$ is the compliance tensor, $\vec{\alpha}$ is the thermal expansion coefficient tensor, $T = T_s - T_0$, V is the sample volume, and S_1 is that part of the laminate surface subjected to a fixed displacement $\hat{u}$ [33]. In this problem S_1 is null. Note that for two-dimensional analysis the stress and thermal expansion coefficient tensors are written as vectors: $\vec{\sigma} = (\sigma_{xx}, \sigma_{zz}, \sigma_{xz})$ and $\vec{\alpha} = (\alpha_x, \alpha_z, \alpha_{xz})$ Substituting the stresses in Eq. (1) into Eq. ($A1$) gives

$$\Gamma = \Gamma_0 + t_1^2\int_{-\rho}^{\rho}\left(C_1\psi^2 + C_2\psi\psi'' + C_3\psi''^2 + C_4\psi'^2 - 2\Delta\alpha T\psi\right)d\xi \qquad (A2)$$

where

$$C_1 = \frac{1}{E_x^{(1)}} + \frac{1}{\lambda E_x^{(2)}} \qquad (A3)$$

$$C_2 = -\frac{\lambda\nu_{xz}^{(1)}}{3E_x^{(1)}} + \frac{\nu_{xz}^{(2)}}{E_x^{(2)}}\left(1 + \frac{2\lambda}{3}\right) \qquad (A4)$$

$$C_3 = \frac{1}{20E_z^{(1)}} + \frac{\lambda}{60E_z^{(2)}}\left(8\lambda^2 + 20\lambda + 15\right) \tag{A5}$$

$$C_4 = \frac{1}{3G_{xz}^{(1)}} + \frac{\lambda}{3G_{xz}^{(2)}} \tag{A6}$$

This expression is identical to the one for $[0_m/90_n]_s$ laminates [9,10] except that the constants are slightly modified to account for the general (S) orthotropic sublaminate in place of the specific $[0_m]$ sublaminate.

Because only the defined constants C_1 to C_4 have new forms, all results expressed in terms of those constants can be applied to both $[(S)/90_n]_s$ and $[0_m/90_n]_s$ laminates. We quote some useful results from Refs. [9] and [10]. $\psi(\xi)$ is given in Eq. (9). Defining $p = (C_2 - C_4)/C_3$ and $q = C_1/C_3$, $\phi(\xi)$ in Eq. (9) has two possible forms depending on the value of $4q/p^2$. When $4q/p^2 > 1$

$$\begin{aligned}\phi(\xi) = &\frac{2(\beta\sinh\alpha\rho\cos\beta\rho + \alpha\cosh\alpha\rho\sin\beta\rho)}{\beta\sinh 2\alpha\rho + \alpha\sin 2\beta\rho}\cosh\alpha\xi\cos\beta\xi \\ &+ \frac{2(\beta\cosh\alpha\rho\sin\beta\rho - \alpha\sinh\alpha\rho\cos\beta\rho)}{\beta\sinh 2\alpha\rho + \alpha\sin 2\beta\rho}\sinh\alpha\xi\sin\beta\xi\end{aligned} \tag{A7}$$

where

$$\alpha = \frac{1}{2}\sqrt{2\sqrt{q} - p} \qquad \text{and} \qquad \beta = \frac{1}{2}\sqrt{2\sqrt{q} + p} \tag{A8}$$

When $4q/p^2 < 1$

$$\phi(\xi) = \frac{\frac{\beta\cosh\alpha\xi}{\sinh\alpha\rho} - \frac{\alpha\cosh\beta\xi}{\sinh\beta\rho}}{\beta\coth\alpha\rho - \alpha\coth\beta\rho} \tag{A9}$$

where

$$\alpha = \sqrt{\frac{-p}{2} + \sqrt{\frac{p^2}{4} - q}} \qquad \text{and} \qquad \beta = \sqrt{\frac{-p}{2} - \sqrt{\frac{p^2}{4} - q}} \tag{A10}$$

In deriving expressions for strain energy and strain energy release rate we used an excess strain energy function, $\chi(\rho)$, and its derivative, $\chi'(\rho)$. From Refs. [5], [6], [9], and [10], $\chi(\rho) = -\phi'''(\rho)$. When $4q/p^2 > 1$

$$\chi(\rho) = 2\alpha\beta\left(\alpha^2 + \beta^2\right)\frac{\cosh 2\alpha\rho - \cos 2\beta\rho}{\beta\sinh 2\alpha\rho + \alpha\sin 2\beta\rho} \tag{A11}$$

$$\chi'(\rho) = 4\alpha\beta\left(\alpha^2 + \beta^2\right)^2\frac{\sinh 2\alpha\rho\sin 2\beta\rho}{(\beta\sinh 2\alpha\rho + \alpha\sin 2\beta\rho)^2} \tag{A12}$$

When $4q/p^2 < 1$

$$\chi(\rho) = \alpha\beta\left(\beta^2 - \alpha^2\right)\frac{\tanh\beta\rho\tanh\alpha\rho}{\beta\tanh\beta\rho - \alpha\tanh\alpha\rho} \tag{A13}$$

$$\chi'(\rho) = \alpha^2\beta^2\left(\beta^2 - \alpha^2\right)\frac{\frac{\tanh^2\beta\rho}{\cosh^2\alpha\rho} - \frac{\tanh^2\alpha\rho}{\cosh^2\beta\rho}}{(\beta\tanh\beta\rho - \alpha\tanh\alpha\rho)^2} \tag{A14}$$

Acknowledgments

This work was supported in part by a contract from NASA Langley Research Center (NAS1-18833) monitored by Dr. John Crews, in part by a gift from ICI Advanced Composites monitored by Dr. J. A. Barnes, and in part by a gift from the Fibers Department of E. I. duPont deNemours & Company monitored by Dr. Alan R. Wedgewood.

References

1. F. W. Crossman and A. S. D. Wang, *ASTM STP* **775** (1982) 118.
2. A. S. D. Wang and R. W. Crossman, *J. Comp. Mat. Supplement* **14** (1980) 71.
3. F. W. Crossman, W. J. Warren, A. S. D. Wang, and G. E. Law, Jr., *J. Comp. Mat Supplement* **14** (1980) 89 .
4. A. S. D. Wang, *Composites Technology Review* **6** (1984) 45.
5. Z. Hashin, *Mechanics of Materials* **4** (1985) 121.
6. Z. Hashin, *Eng. Fract. Mech.* **25** (1986) 771.
7. Z. Hashin, *J. Appl. Mech.* **54** (1987) 872.
8. Z. Hashin, *Composites Science and Technology* **31** (1988) 247.
9. J. A. Nairn, *J. Comp.Mat.* **23** (1989) 1106. (*Errata* published as *J. Comp. Mat.* **24** (1990) 233).
10. S. Liu and J. A Nairn., *J. Reinforced Plastics and Comp.* (1991) submitted.
11. S. Liu and J. A. Nairn, *Proceedings of the Fifth Annual Meeting of the American Society of Composites* (1990) 287.
12. S. Liu and J. A. Nairn, unpublished results.
13. T. K. O'Brien, *ASTM STP* **876** (1985) 282.
14. T. K. O'Brien, *ASTM STP* **1059** (1990) 7.
15. S. A. Salpekar and T. K. O'Brien, NASA TM 102591 (1990).
16. L. R. Dharani and H. Tang, *Int. J. Fract.* **46** (1990) 123.
17. J.C. Fish and S. W. Lee, *ASTM STP* **1059** (1990) 271.
18. A. S. D. Wang, N. N. Kishore and C. A. Li, *Composites Science and Technology* **24** (1985) 1.
19. G. C. Sih, P. C. Paris, and G. R. Irwin, *Int. J. Fract.* **1** (1965) 189.
20. K. Palaniswamy and W. G. Knauss, in *Mechanics Today, Vol. 4*, Pergamon Press, Oxford (1978).
21. S. Mostovoy and E. J. Ripling, *J. Appl. Polym. Sci.* **10** (1966) 1351.
22. T. K. O'Brien, *ASTM STP* **775** (1982) 140.
23. K. W. Garrett and J. E. Bailey, *J. Mat. Sci.* **12** (1977) 157.
24. K. L Reifsnider, *Proc. 14th Ann. Mtg of SES*, Lehigh, PA, November, 1977.
25. P. W. Manders, T. W. Chou, F. R. Jones, and J. W. Rock, *J. Mat. Sci.* **19** (1983) 2876.
26. D. L. Flaggs, *J. Comp. Mat.* **19** (1985) 29.
27. H. Fukunaga, T. W. Chou, P. W. M. Peters, and K. Schulte, *J. Comp. Mat.* **18** (1984) 339.
28. Y. M. Han, H. T. Hahn, and R. B. Croman, *Comp. Sci. & Tech.* **31** (1987) 165.
29. N. Laws and G. J. Dvorak, *J. Comp. Mat.* **22** (1988) 900.
30. R. J. Nuismer and S. C. Tan, *J. Comp. Mat.* **22** (1988) 306.
31. J. A. Nairn and S. Hu, Micromechanics of Damage: A Case Study of Matrix Microcracking, in: R. Talreja, ed., *Damage Mechanics of Composite Materials* (1991) submitted.
32. J. A. Nairn and S. Hu, *Eng. Fract. Mech.* (1990) submitted.
33. Carlson, D. M., Linear Thermoelasticity, in: C. Truesdall, ed., *Mechanics of Solids: Volume II*, Springer-Verlag, Berlin (1984) 325.